JOURNAL OF MATERIALS SCIENCE 31 (1996) 843–849

Topographic study of superplastically formed AA7475 hemispherical domes

M. G. ZELIN*
Department of Chemical Engineering and Materials Science, University of California, Davis, CA 95616, USA

Sliding of grain groups occurs during superplastic stretching of 7475 aluminium alloy with a spherical punch. Such co-operative grain boundary sliding (CGBS) is accompanied by cavity formation in intersection sites of CGBS surfaces, formation of striated bands and migration of sliding grain boundaries. Fibres were observed evolving from the striated bands between grains separated due to CGBS. This fibring process anticipates extreme ductility of the material and could be considered as "microsuperplasticity" originating from operation of a diffusion-like process or incipient melting.

1. Introduction

A study of the topographic features of deformation relief occurring on prepolished surfaces during deformation provides important information on the deformation mechanisms operating. Studies performed on a wide variety of superplastic (SP) materials have shown grain boundary sliding (GBS) to be a major process of SP flow [1]. Recently [2–4], the co-operative manner of GBS, i.e. sliding of grain groups, has been reported. Predominantly, occurrence of GBS under uniaxial tension has been studied. However, commercial application of superplastic flow incorporates more complex stress–strain states, e.g. a biaxial stress–strain state in the case of sheet forming.

The objective of this paper was examination of the surface topography of superplastically stretched 7475 aluminium alloy hemispherical domes, with emphasis on the study of the GBS group character. An understanding of the surface quality limits after SP forming adds to the importance of this study; particularly, because, surface roughness may originate from co-operative GBS [5].

2. Experimental procedure

A 7475 aluminium alloy sheet material, 1.5 mm thick, with an average grain size of 10 μm was obtained from Kaiser Aluminum and Chemical, Co. The material exhibits superplastic behaviour [6] (total elongation to failure under uniaxial tension was 1000%) at 515 °C and a strain rate, $\dot{\varepsilon}$, of $2 \times 10^{-4}\,s^{-1}$. Square blanks, $50 \times 50\,mm^2$ were mechanically polished, with final polishing on 0.3 μm alumina. Two sets of marker lines were inscribed along and perpendicular to the rolling direction, using a diamond paste with a particle size of 3 μm.

Tests were conducted in a four-post MTS machine. A stainless steel die assembly and a hemispherical punch, with a diameter of 30 mm, were used. A radial heating furnace, with a thermocontroller providing a stable temperature within ± 3 °C, was used. The heating time was 90 min, and the soaking time was 30 min. Tests were performed under a constant velocity ram movement, v, equal to $4.3 \times 10^{-4}\,mm\,s^{-1}$. Analysis of the dependence of strain rate as a function of punch displacement, which was derived assuming uniform deformation thickness (see Appendix), showed that actual strain rates were close to the optimal strain rate, $\dot{\varepsilon} = 2 \times 10^{-4}\,s^{-1}$.

Deformed domes were studied in a scanning electron microscope (SEM). Chemical analysis was performed using a microprobe with a beam spot of 1 μm in diameter.

3. Results and discussion

Mechanical behaviour, typical of stretching [7], was observed: load increased with increasing punch displacement.

Fig. 1a–c shows typical SEM micrographs taken from different regions of the dome, with locations indicated by letters a–c in the inset given in Fig. 1a. Fig. 1d–f demonstrates regions designated by crosses in Fig. 1a–c under higher magnification. New grain facets became visible due to displacement of grains, with respect to each other, in all regions. This displacement of grains and offset of marker lines at grain boundaries indicate intensive grain boundary sliding. The heights of steps formed as a result of GBS and marker line offsets increases towards the top of the dome. The lengths of marker line segments, in which marker lines were broken due to sliding and which reflect the group size of grains sliding as blocks,

Present address: Concurrent Technologies Corporations, 1450 Scalp Avenue, Johnstown, PA 15904, USA.

0022–2461

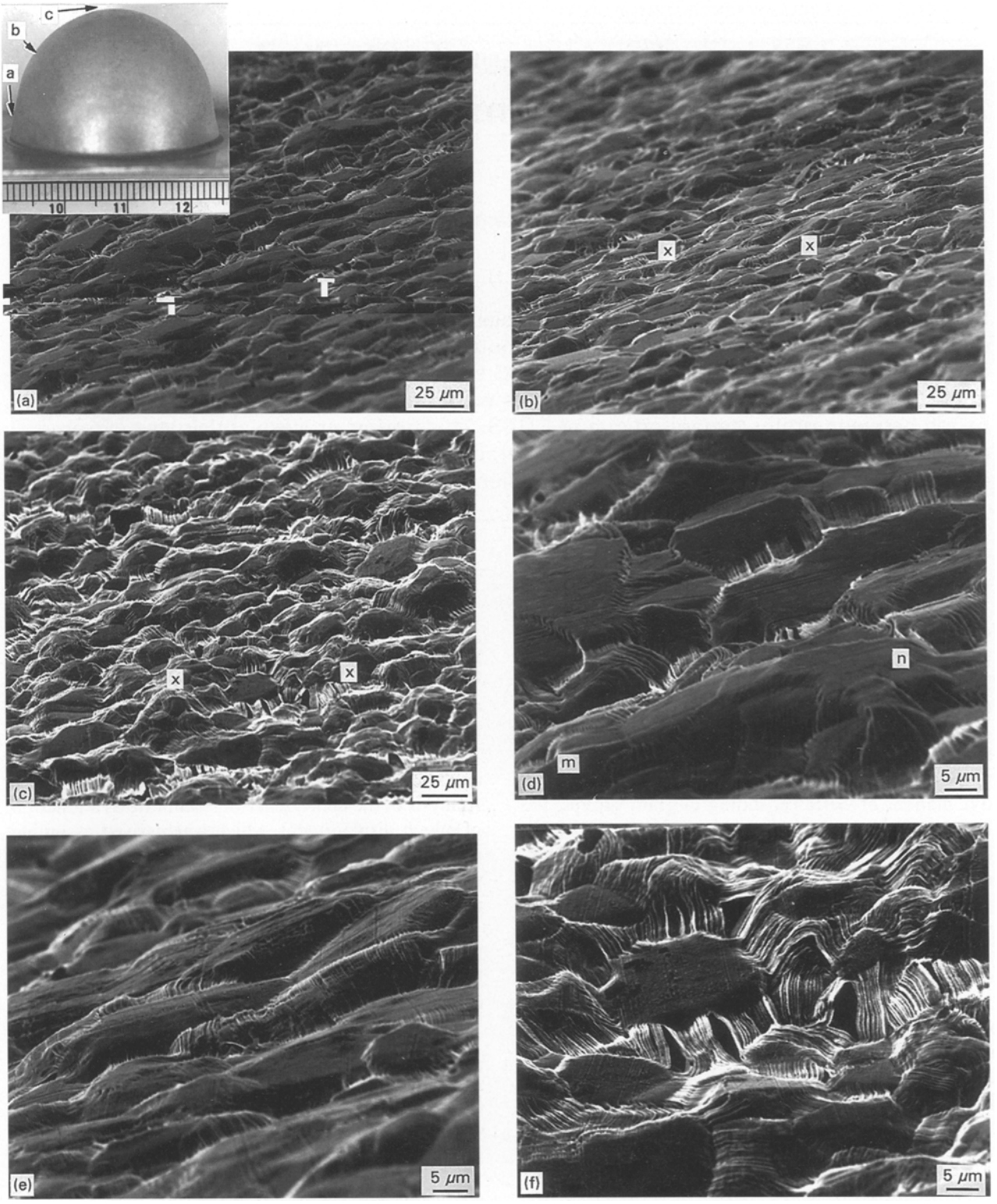

Figure 1 (a)–(c) SEM micrographs taken from the prepolished surface of 7475 alloy in different regions (indicated by the corresponding letters in the inset given in Fig. 1a) of superplastically stretched spherical dome. (d)–(f) Show regions designated by crosses in Fig. 1a–c under higher magnification.

decrease towards the top of the dome. Such groups of grains, inside which marker lines are undisturbed or distorted slightly (for instance marker line segment m-n in Fig. 1d), are clearly seen near the base of the dome. The fact that the length of unbroken marker line segment decreases towards the top of the dome indicates that more grains became involved in GBS. Meanwhile, the group character of GBS is also observed in regions close to the dome top. Such groups of grains sliding as an entity are seen in Fig. 2a. They are surrounded by shear surfaces which are decorated by wide striated bands [8, 9], e.g. see groups of grains designated by letters P and R in Fig. 2a. The striated bands form long chains. Wedge-like features are seen at sites where surfaces of co-operative GBS (CGBS), i.e. grain group sliding meet each other. In certain instances, cavity formation occurs at the intersection of CGBS surfaces (arrowed in Fig. 2a and shown under high magnification in Fig. 2b). Such wedge-like features are clearly seen in Fig. 2c. They are formed by

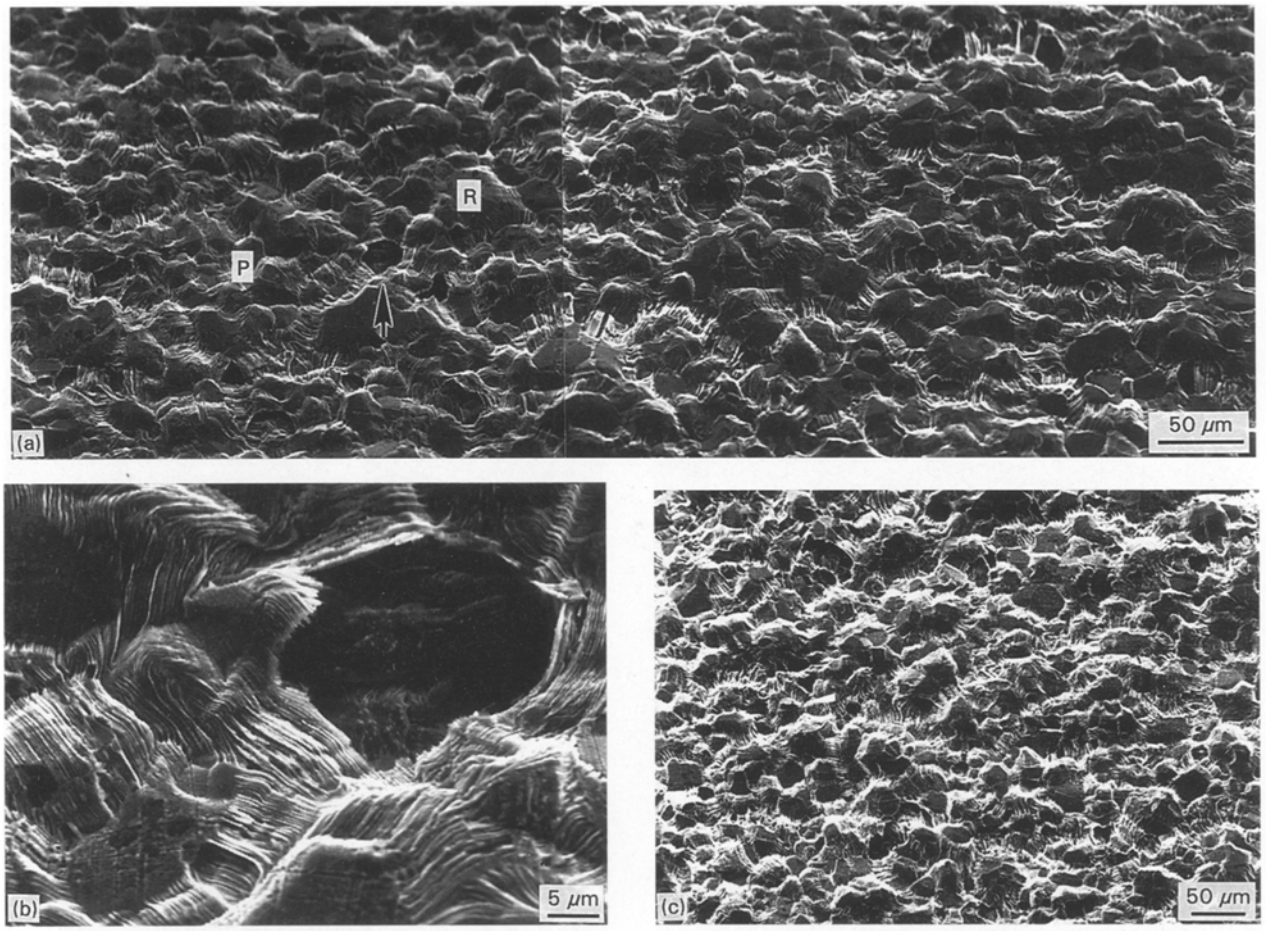

Figure 2 SEM micrographs illustrating the group manner of GBS (a), cavity formation at the intersections of CGBS surfaces (b), and wedge-like features (c) in the region close to the top of superplastically stretched 7475 alloy spherical dome. An arrow in Fig. 2a points to the cavity shown in Fig. 2b under higher magnification.

CGBS surfaces, which appear very bright in the SEM micrographs because of extensive secondary electron emission from the steps, and striations originating due to GBS.

Significant grain boundary sliding at CGBS surfaces is accompanied by grain boundary migration and formation of fibres evolving from striated bands (Fig. 3a–d). The traces of migrating grain boundaries are seen as bright–dark fringes (arrowed in Fig. 3b) at which the marker line becomes stepped (Fig. 3c). Striations at sliding grain boundaries are consistent with the direction of GBS (see an inset in the lower left corner in Fig. 3c). Cavities of triangular shape, formed due to GBS, are often observed at triple points. These cavities are easy to distinguish from those introduced by mechanical polishing (despite all precautions taken, the presence of some cavities over quite a large area of blanks was caused by fracture and pull out of brittle particles during polishing). Cavities originating from mechanical polishing have very irregular shape with sharp edges and are located most often inside grains (arrowed in Fig. 3d). Cavities formed due to GBS have round corners, and in many instances there are fibres connecting grains separated due to CGBS (Fig. 3d). Grains situated in underlying layers become exposed when such big cavities are formed. Striations are seen at the grain boundaries of freshly exposed grains, thereby indicating that these features are typical not only of grains located at the original surface, but of grains emerging from the bulk as well. The same applies to the precipitates which were observed both in the grains located at the original surface and in the grains emerging from the bulk. Chemical analysis showed Zn and Mg as the major elements comprising the precipitates.

Fig. 4 presents additional evidence of the features described above, which can be summarized as follows

1. Sliding of grain groups takes place (see blocks of grains designated by letters K, M and N in Fig. 4a).
2. There is a significant offset of marker lines at surfaces of co-operative GBS (see the inset given in the left lower corner in Fig. 4b).
3. Cavity formation at the intersection of CGBS surfaces is often observed (Fig. 4a, arrowed).
4. Interim positions of migrating grain boundaries are seen as bright/white steps in Fig. 4b, c.
5. Fibres at sliding boundaries, which form CGBS surfaces (Fig. 4d), are observed.

Comparison of the features present at the surface of biaxially deformed material with those observed in experiments in uniaxial tension shows that there are many common features to the occurrence of GBS under uniaxial and biaxial deformation states. The co-operative manner of GBS, reported in a number of SP materials deformed under uniaxial tension [2–5] and in shear [10], was observed in this study, as well as co-operative grain boundary migration [11]. Fibres similar to those demonstrated by Figs 3 and 4 have

been reported recently [12, 13]. However, there are certain differences between the occurrence of GBS under uniaxial tension and biaxial deformation.

1. There is significant displacement of grains in a direction normal to the sheet plane (see Fig. 1). This is a result of differences in the deformation strain states. The ratio of strain thickness, ε_t, to effective strain, ε_e, is $\varepsilon_t/\varepsilon_e = 0.5$ under uniaxial conditions, while $\varepsilon_t/\varepsilon_e = 1$ for the biaxial strain state.

2. Fibres reported in [12, 13] were observed at the fracture surface. In this study, fibres were observed at the deformed surface. The fibres were seen at grain facets exposed due to GBS when grain displacements were significant, i.e. at grain boundaries which form CGBS surfaces. At lower strain levels, grain boundary facets exhibited striation bands [12, 13]. This indicates that fibres observed in this study evolved from striated bands, as schematically illustrated by Fig. 5a. The mechanism of evolution of striations into fibres is not clear. Evidently, formation of the fibres indicates extreme local plasticity of the material. However, such microsuperplasticity [12] must have a different origin

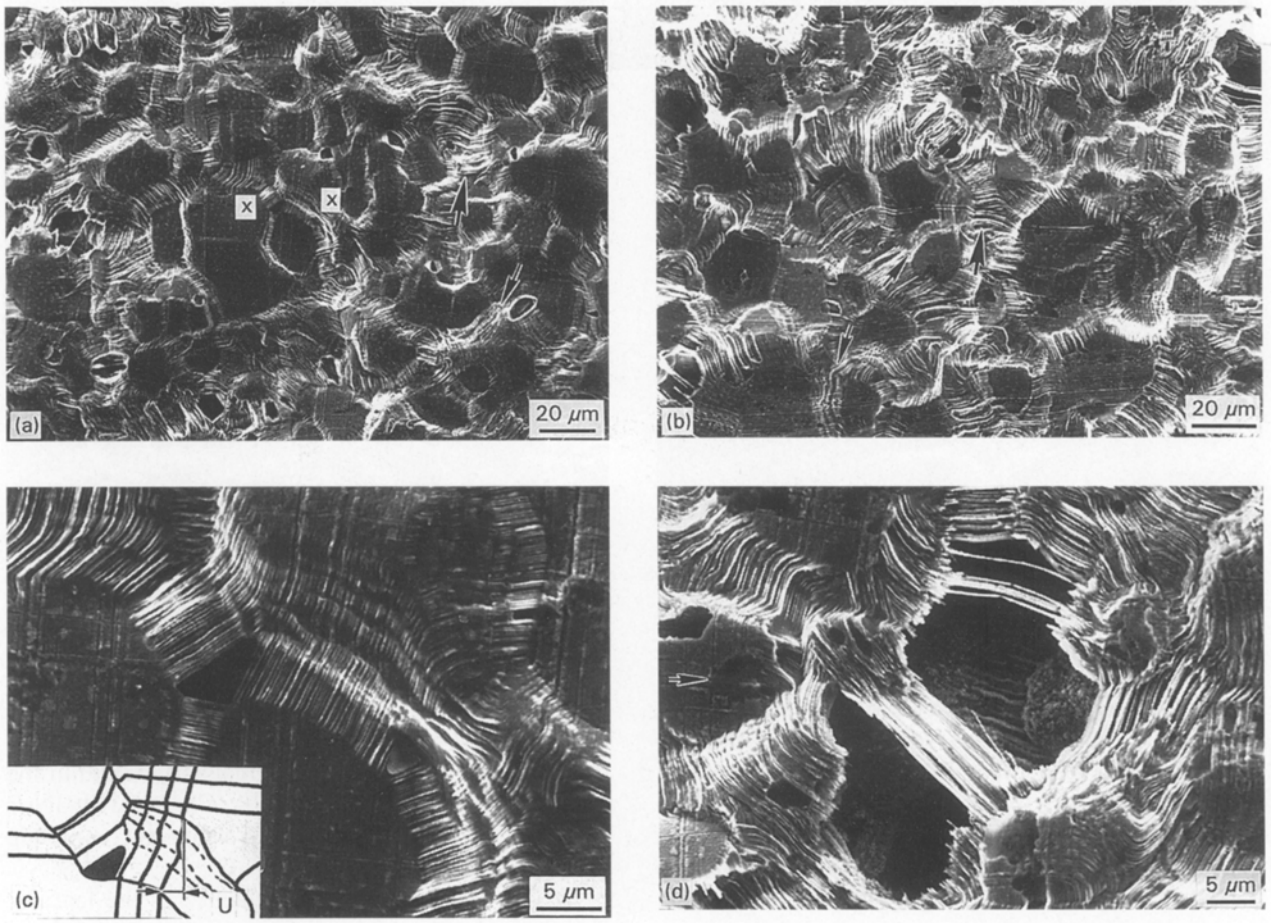

Figure 3 SEM micrographs showing traces of grain boundary migration, striated bands (arrowed in Fig. 3a, b with small arrows and big arrows, respectively), and fibres (d) observed at the CGBS surfaces. (c) Shows the region designated by crosses in Fig. 3a under higher magnification and illustrates the same directionality in offsets of marker lines and striations (see inset).

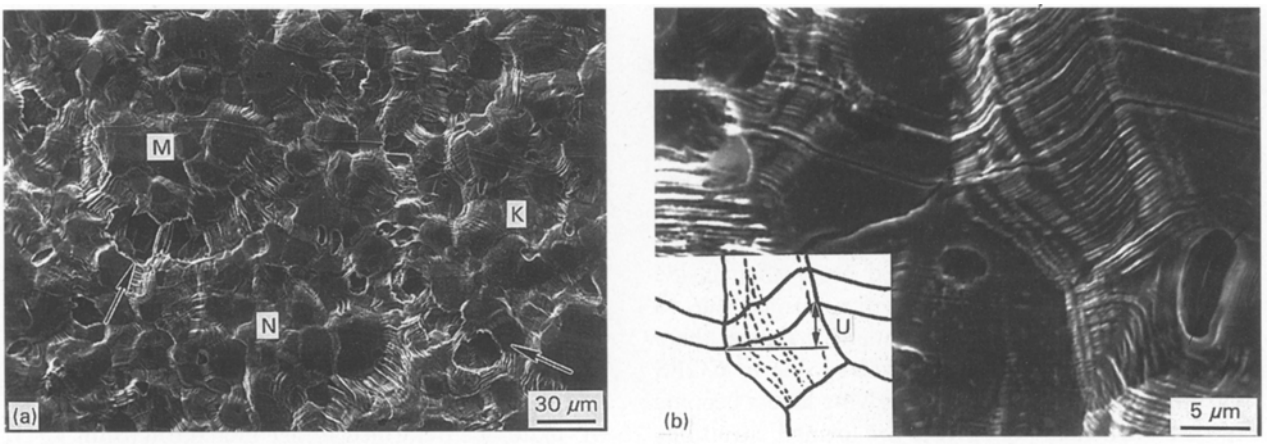

Figure 4 SEM micrographs of (a) groups of grains sliding as an entity (designated by letters K, M and N), (b) offset of marker lines at grain boundaries (see inset), (c) interim positions of migrating grain boundary, and (d) fibres observed as a result of CGBS in superplastically 7475 spherical dome.

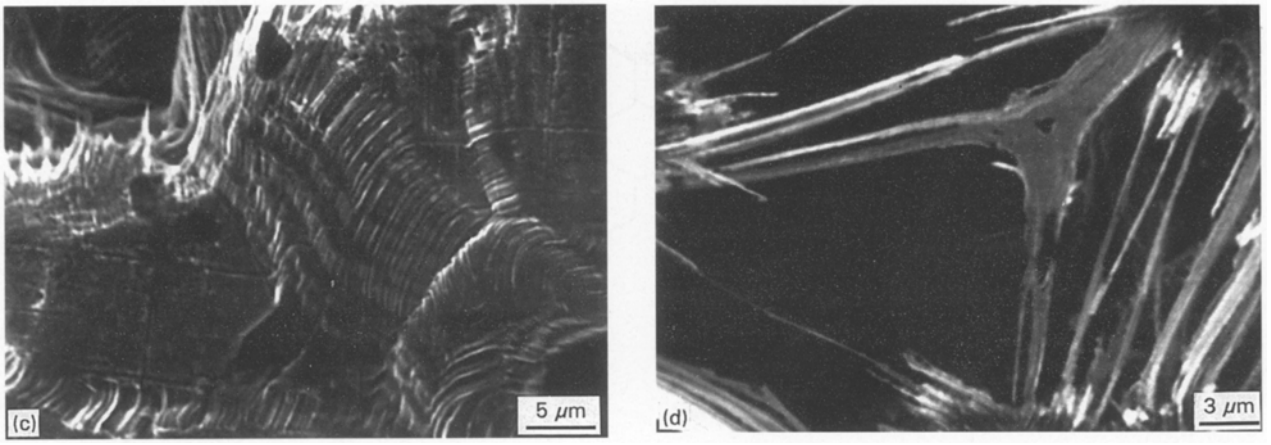

Figure 4 (Continued).

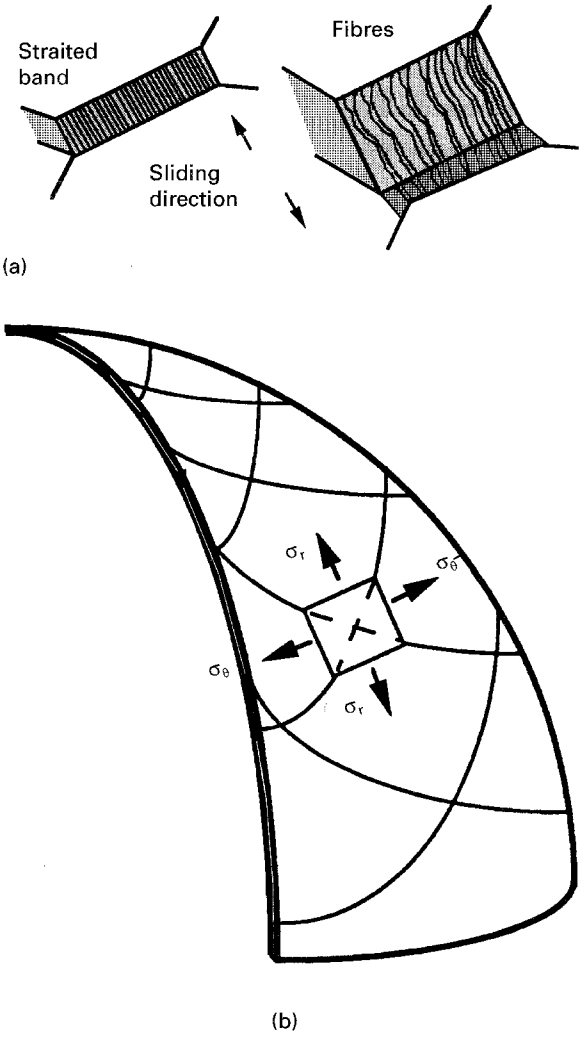

Figure 5 Schematic illustrations of evolution of striated bands into fibres (a) and the pattern of slip lines in a sheet subjected to stretching by a spherical punch (b).

from that of superplastic flow. Indeed, the diameter of fibres is less than 1 μm, which eliminates GBS from the list of possible mechanisms for fibring, since the grain size in the bulk was 10 μm. It is also improbable that fibre formation can be a result of the operation of dislocation slip. The appearance of fibres allows one to suggest their diffusion related nature. This is in consequence to the important role of diffusion creep in the formation of striated bands [9] from which the fibres evolve. Note that incipient melting at low temperature eutectic and/or dehydrogenization [14] could also cause fibre formation.

It has been shown [10] that the macroscopic manner of CGBS can be assessed based on slip line field theory [15]. Indeed, the slip line field theory predicts the surface pattern of maximum shear stress. Since GBS occurs under shear stress traction, one can expect extensive GBS at the grain boundaries to be aligned with the direction of maximum shear stress. The surfaces of maximum shear stress form 45° with respect to the directions of principal stress [15]. Normal stresses in forming a thin sheet are close to zero, and radial and circumferential stresses may be suggested to be the principal stresses involved [16]. Fig. 5b illustrates the pattern of slip lines for the case of a spherical dome, which is consistent with that of macroscopic shear surfaces observed experimentally.

A number of topological models have been proposed in order to explain geometrical aspects of SP flow progress. However, models similar to those proposed by Ashby and Verrall [17] and by Gifkins [18] were developed to explain grain rearrangement during SP under uniaxial tension and they do not reflect grain movement under a biaxial strain state. Both Ashby–Verrall's model [17] and Gifkins' model [18] can be modified as shown in Fig. 6a, b, respectively, in order to explain the decrease in sheet thickness. Neither of the models reflect grain rearrangement in the sheet plane: Ashby–Verrall's model [17] does not account for surface area increases, and there is a loss of contact between all four grains in Gifkins' model [18] (gaps between grains are shown as solid black in Fig. 6c). Note that in the last case, the suggestion [19] of exposing new grain facets (grey regions between the grains going apart in Fig. 6d) allows one to avoid the problem of grain separation (Fig. 6d). Still, the situation shown in Fig. 6d, which is close to Langdon's model [19], reflects only a particular case where the spacing of shear surfaces is equal to grain size.

Generally, the spacing of shear surfaces may be more than the grain size, and sliding of groups of grains takes place (Figs 1–4). Fig. 6e illustrates schematically an early stage of such a CGBS process. It suggests that sliding starts at grain boundaries which

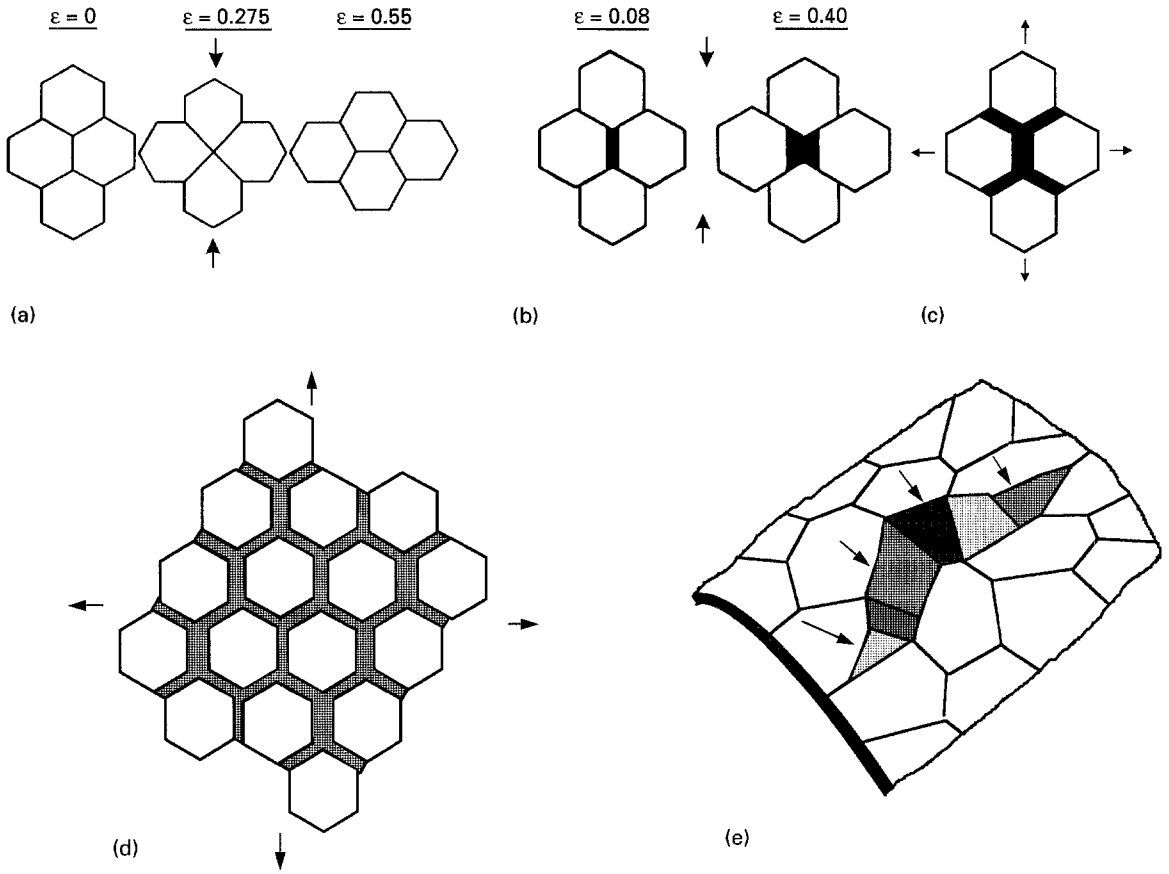

Figure 6 Modified geometrical SP models of (a) Ashby–Verrall [17] (b), Gifkins [18], and (d) Langdon [19], explaining through thickness strain and in-plane strain in a biaxially deformed SP sheet, respectively. (c) Illustrates grain separation if Gifkins' model [18] is used to describe grain rearrangement in the sheet plane; (e) schematic illustration of grain group sliding.

are more prone to slide and their orientation is close to the orientation of the maximum shear stress. Shear propagates in the direction indicated by the arrows in Fig. 6e at grain boundary facets which form a CGBS surface, and results in an increase in the area of the sheet surface and in a decrease of the sheet thickness as well. Observed wedge-like features (Fig. 2a, c), which can be formed both as a result of CGBS initiation and intersection of two CGBS surfaces, support the suggested schematics of CGBS (Figs 5b and 6e).

4. Conclusions

1. Co-operative grain boundary sliding (CGBS), i.e. sliding of grain groups, takes place during superplastic bulging of a 7475 aluminium alloy with a spherical punch.

2. There is much in common between the progress of grain boundary sliding under uniaxial and biaxial strain states; for instance, coupling of CGBS and co-operative grain boundary migration, formation of striated bands at grain boundary facets exposed due to CGBS, cavity formation in intersection sites of CGBS surfaces, etc. Qualitatively, the difference in occurrence of grain boundary sliding under uniaxial and biaxial deformation states relates to the ratio of the strain component normal to the sheet plane to the effective strain.

3. Formation of fibres at grain boundary facets at which CGBS took place has been observed. These fibres evolve from striated bands. Diffusion or incipient melting type processes can be suggested as mechanisms for this kind of "microsuperplasticity".

4. Geometrical models of superplasticity considering grain boundary sliding of individual grains do not explain strain accumulation under biaxial deformation states. The results of experimental observations on the macroscopic scale and on the scale of grain groups can be interpreted in terms of CGBS.

Appendix

In order to obtain the dependence of the effective strain rate as a function of spherical punch displacement during stretching, it is assumed that the deformed portion of the blank can be considered as a segment of a sphere of uniform thickness (Fig. A1). The effective strain rate at the top of the sphere is determined as

$$\dot{\varepsilon} = \dot{A}/A$$

The area of the spherical segment is determined as

$$A = 2\pi Rh$$

where R is the radius of the dome and h is its height. It is evident from Fig. A1 that

$$R = r/\sin\alpha$$

where r is the radius of the die.

An angle α can be expressed through h and r as

$$tg\alpha/2 = h/r$$

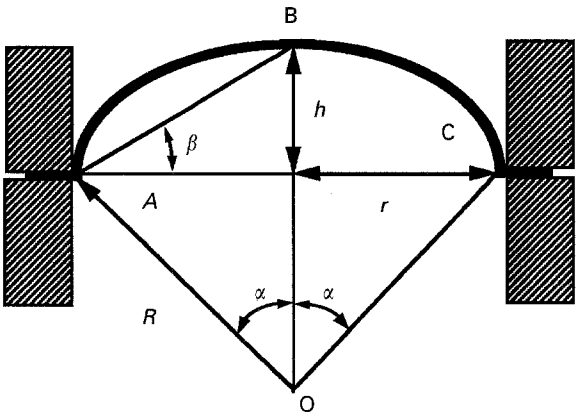

Figure A1 Schematic diagram illustrating the geometry of sheet deformed by a spherical punch.

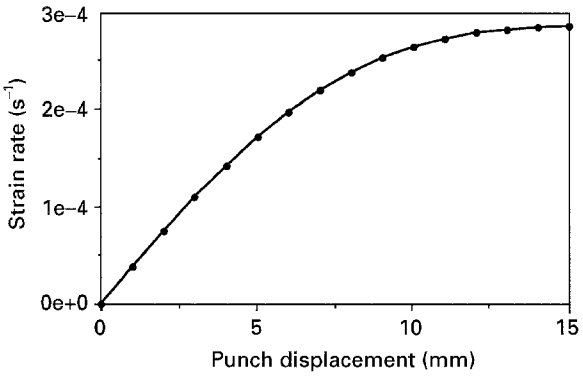

Figure A2 Changes in effective strain rate, $\dot{\varepsilon}$, during stretching of a blank with a spherical punch as a function of punch displacement, h.

The last expression comes from the fact that angles α and β have the same arc BC, and the angle AOB = BOC = α is the central angle, while the angle BAC = β is a circumscript angle. Then

$$\sin\alpha = 2rh/(r^2 + h^2)$$

and

$$A = 2\pi rh/\sin\alpha = \pi(r^2 + h^2)$$

Finally, for strain rate

$$\dot{\varepsilon} = 2h\dot{h}/(r^2 + h^2) = 2hv/(r^2 + h^2)$$

where v is the punch velocity.

Fig. A2 shows the dependence of strain rate as a function of punch displacement for a ram velocity, $v = 4.3 \times 10^{-4}$ mm s^{-1}. The actual strain rate varies in a range which is close to the optimal SP strain rate $\dot{\varepsilon} = 2 \times 10^{-4}$ s^{-1}.

Acknowledgements

This work was supported by a grant (No. DMR-93-00217) from the US National Science Foundation. The author wishes to thank Professor A. K. Mukherjee for his valuable discussion and support, Dr A. T. Male for his comments and Dr H. S. Yang for providing the material.

References

1. J. PILLING and N. RIDLEY " Superplasticity in Crystalline Solids" (The Institute of Metals, London, 1989) p. 240.
2. M. G. ZELIN and A. K. MUKHERJEE *J. Mater. Sci. Lett.* **13** (1994) 1258.
3. V. V. ASTANIN, O. A. KAIBYSHEV and S. N. FAIZOVA, *Acta Metall. Mater.* **42** (1994) 2617.
4. M. G. ZELIN and A. K. MUKHERJEE *J. Mater. Sci.* **28** (1993) 6767.
5. M. G. ZELIN, T. BIELER and A. K. MUKHERJEE, *Metall. Trans.* **24A** (1992) 1209.
6. H. S. YANG, Internal report, (Kaiser Aluminum & Chemical Co., Pleasonton, CA, 1994).
7. E. D. MIELNIK, "Metalworking Science and Engineering" (McGraw-Hill, New York, 1991) p. 738.
8. W. A. BACKOFEN, G. S. MURTY and S. W. ZEHR, *Trans. Metall. Soc. AIME* **242** (1968) 329.
9. I. I. NOVIKOV, V. K. PORTNOY and V. S. LEVCHENKO, *Acta Metall.* **29** (1981) 1077.
10. M. ZELIN, M. DUNLAP, A. ROSEN and A. K. MUKHERJEE, *J. Appl. Phys.* **74** (1993) 4972.
11. M. ZELIN, R. JAMES and A. K. MUKHERJEE, *J. Mater. Sci. Lett.* **12** (1993) 176.
12. W. J. D. SHAW, *Mater. Lett.* **4** (1985) 1.
13. T. IMAI, G. L'ESPERANCE and B. D. HONG, *Scripta Metall. Mater.* **31** (1994) 321.
14. C. C. BUMPTON and J. W. EDINGTON, *Metall. Trans.* **13A** (1982) 1721.
15. A. NADAI, "Theory of Flow and Fracture of Solids", Vol. 1 (McGraw-Hill, New York, 1950) p. 320.
16. A. D. TOMLYENOV, "Theory of Plastic Deformation of Metals", (Metallurgy, Moscow, 1972) p. 232.
17. M. F. ASHBY and R. A. VERRALL, *Acta Metall.* **21** (1973) 149.
18. R. C. GIFKINS, *J. Mater. Sci.* **13** (1978) 1926.
19. T. G. LANGDON, *Metals Forum* **4** (1981) 14.

Received 2 Feburary
and accepted 11 May 1995